Journal of $CO_2$ Utilization 40 (2020) 101218

Contents lists available at ScienceDirect

Journal of $CO_2$ Utilization

journal homepage: www.elsevier.com/locate/jcou

# Magnetic carbon nanotubes: Carbide nucleated electrochemical growth of ferromagnetic CNTs from $CO_2$

Xirui Wang[a], Farbod Sharif[b], Xinye Liu[a], Gad Licht[b], Matthew Lefler[a], Stuart Licht[a,*]

[a] Dept. of Chemistry, George Washington University, Washington DC, 20052, USA
[b] C2CNT Corp, 1035 26 St NE, Calgary, AB, T2A 6K8, Canada

ARTICLE INFO

*Keywords:*
Carbon nanotubes
Magnetic carbon nanomaterials
Carbon dioxide electrolysis
Molten carbonate
Greenhouse gas mitigation

ABSTRACT

This study demonstrates that $CO_2$ can be split by molten carbonate electrolysis (1) to grow magnetic carbon nanotubes (CNTs) and (2) that the process can be initiated by carbide nucleation points acting as growth catalysts. This opens the path to other similar electrochemically prepared magnetic carbon nanomaterials. Magnetic carbon nanomaterials have a variety of applications, such as in directing medical therapy to localized regions and recoverable catalysts. In the presence of an iron or nickel containing case to house the molten carbonate electrolysis, or the presence of Fe or Ni in the electrochemical components, ferromagnetic CNTs can grow at the cathode. For example, EDS elemental analysis confirms the presence of iron in the CNTs, and XRD confirms the presence of iron carbide at the CNT nucleation site. The observed interlattice spacing of 0.20 nm of the iron carbide is distinct from the observed 0.36 nm graphene lattice spacing of the CNT walls. An excess iron release can be facilitated into the electrolyte using an iron rich alloy anode, such as Incoloy. The excess iron results in graphene layer coated iron carbide nodules on the exterior of the carbon nanotube product formed at the cathode, as well as iron carbide within these CNTs as observed by SEM and TEM.

## 1. Introduction

Multiwalled carbon nanotubes consist of concentric walls of cylindrical graphene sheets. Graphene was produced and identified in 2004 and is regularly described as a novel 2-D honeycomb-structured material formed by a single layer of $sp^2$ hybrid orbital carbon atoms [1,2]. Its thickness is about 0.335 nm, corresponding to the thickness of one carbon atom, or the distance between two layers of graphene in graphite. Carbon nanotubes (CNTs) have the highest measured tensile strength (strength 93,900 MPa) of any material [3,4]. CNTs have other useful properties including high electrical and thermal conductivity, flexibility, and in addition have the capability to be chemically modified. This has led to a steady rise in their applications: ranging from lightweight structural composites including cement, aluminum, and steel admixtures [5], drug delivery and medical application [6,7], electronics and energy storage [8–12], sensors and analytical chemistry [13,14], resins and polymers [15–19] and textiles [20], to hydrogen storage [21] and water treatment [22,23].

The principle method by which CNTs are produced is chemical vapor deposition, CVD [24,25]. However, the CVD of CNTs is expensive and has a high carbon footprint [26]. A less expensive source of CNTs, will accelerate its market usage. Additionally, if one uses $CO_2$ as a reactant to generate a value-added product such as carbon nanomaterials, this provides impetus to consume this greenhouse gas to mitigate climate change.

A 750 °C molten $Li_2CO_3$ electrolyte in contact with the current 0.041 % $CO_2$ in the air, contains an equilibrium concentration of lithium oxide of 0.2 molal in accord with [13]:

$$Li_2CO_{3(molten)} \rightleftharpoons Li_2O_{(dissolved)} + CO_{2(gas)} \quad (1)$$

In 2013, we introduced the low voltage splitting of $CO_2$ directly to CNTs by electrolysis in molten carbonate solutions in 2013 [27], and in 2015 and thereafter described the production of uniform CNTs and carbon nanofiber product at high coulombic efficiency [5,28–37]. $CO_2$ from the air is directly converted to CNTs as determined by isotope ($^{13}C$) tracking [29]. The electrolytic splitting of $CO_2$ in molten carbonates can occur at electrolysis potentials less than 1 V [30]. The $CO_2$ molten carbonate to Carbon NanoTube process has been termed C2CNT. This electrolytic process can occur as direct carbon capture and conversion from the air without $CO_2$ pre-concentration, with exhaust gas $CO_2$, or with concentrated $CO_2$. By variation of the electrolysis configuration the process can produce in addition to conventional morphology CNTs, doped CNTs, extended CNTs, nanofibers, other carbon nanomaterials including carbon nano-onions, carbon platelets

* Corresponding author.
*E-mail address:* slicht@gwu.edu (S. Licht).

https://doi.org/10.1016/j.jcou.2020.101218
Received 12 May 2020; Received in revised form 12 June 2020; Accepted 13 June 2020

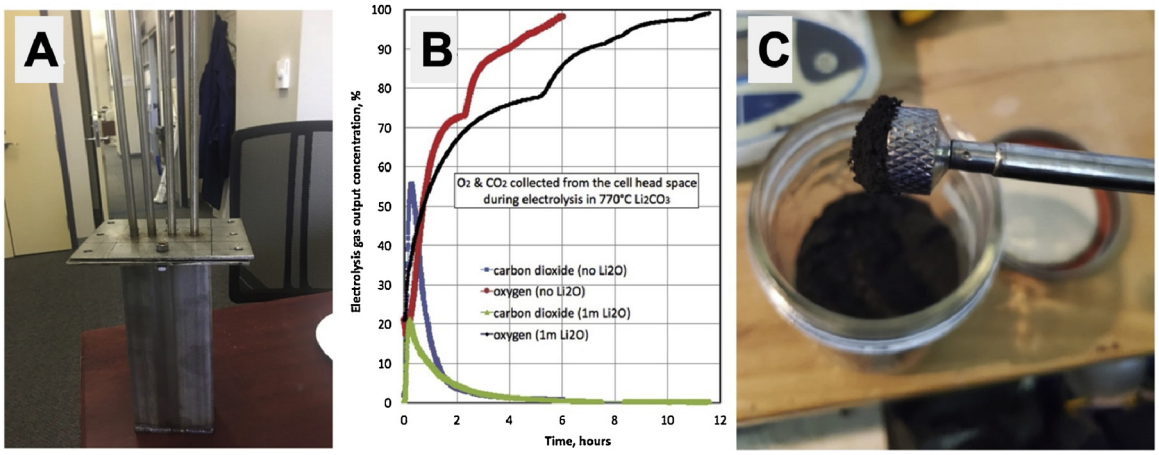


**Fig. 1.** Oxygen evolution during $CO_2$ molten carbonate electrolysis and magnetic carbon nanotubes. (A) Stainless steel electrolysis cell. (B) Oxygen (red) and $CO_2$ (blue) composition of the output gas during the electrolysis [33]. (C) The cathode electrolysis product under many such molten carbonate electrolysis conditions contains carbon nanomaterials, and as shown when grown in an iron containing electrolysis case, or generally in an electrolytic environment containing iron or nickel is strongly attracted to a magnet. The product can be highly uniform magnetic carbon nanomaterials, including magnetic carbon nanotubes (MCNTs).

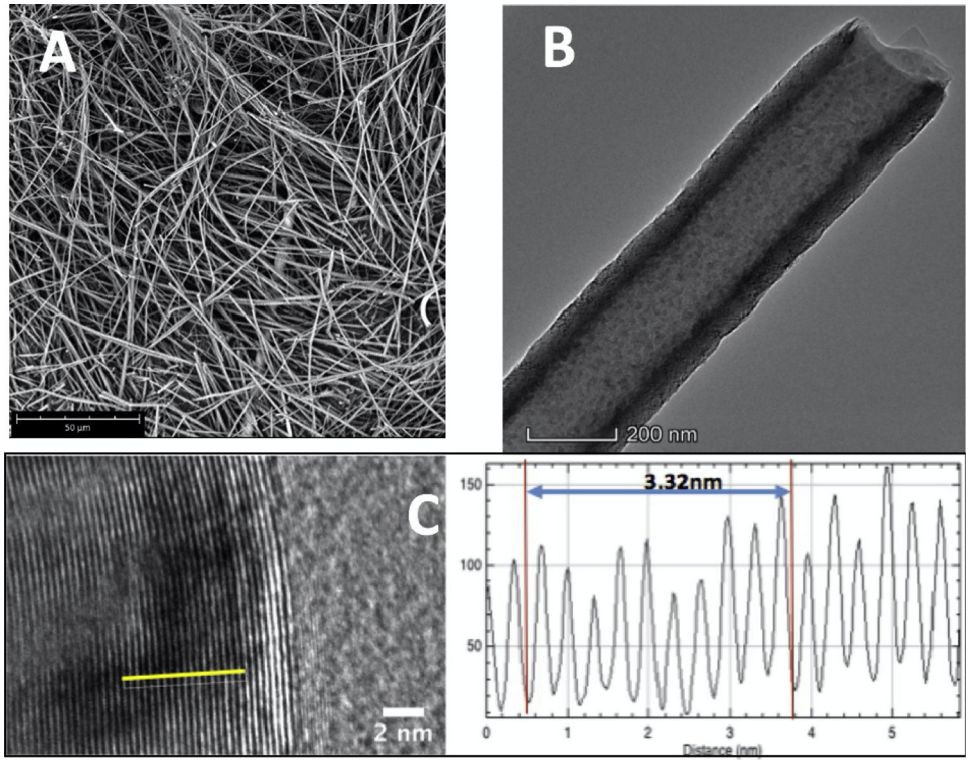


**Fig. 2.** (A) SEM and (B and C) TEM images of CNT cathode product from electrolysis of 5 $cm^2$ Inconel 718 anode and brass cathode in 24-hr equilibrated $Li_2CO_3$ electrolyte. The scale bars are 40 μm in panel A and are respectively 200 and 2 nm in panels B and C.

and graphene [31,29–36]. The synthesis of carbon nanomaterials from $CO_2$ has been of growing interest [37–46].

In the process of $CO_2$ molten carbonate electrolysis, small transition metal "seeds" were observed at the ends of the CNT product, and it was shown that the mechanism of molten carbonate CNT growth is activated by both tip and root transition metal nucleation processes [28,32]. CNTs have been demonstrated in lithiated carbonate electrolytes including pure molten $Li_2CO_3$ (melting point 723 °C), or $Li_2CO_3$ mixed with other carbonates such as $Na_2CO_3$, $K_2CO_3$, $MgCO_3$, $CaCO_3$, $BaCO_3$, or $Li_2CO_3$ mixes with other salts including oxides, borates, sulfates, phosphates or nitrates [28,31,34]. Interestingly, all initial studies of molten carbonate synthesized CNTs assumed a transition metal nucleation seed as the starting point of CNT and did not observe that CNTs synthesized from molten carbonate could be ferromagnetic.

The physical chemical environment of the conventional CVD preparation of CNTs is different than that of the new C2CNT synthesis in most aspects. The latter is an electrochemical process, while the former is chemical. The latter utilizes $CO_2$ and occurs at the liquid/solid interface, while the former utilizes organics as the reactant and generally occurs at a gas/solid interface. There are also significant subtle differences. C2CNT provides a higher density of reactive carbon (the molten carbonate electrolyte) near the growth interface, and while an electric field may, or may not, be applied to the substrate during CVD CNT growth, there is always an intense electric field rapidly decreasing through the double layer adjacent to the cathode during C2CNT growth. Both CVD and C2CNT had been associated with the transition metal

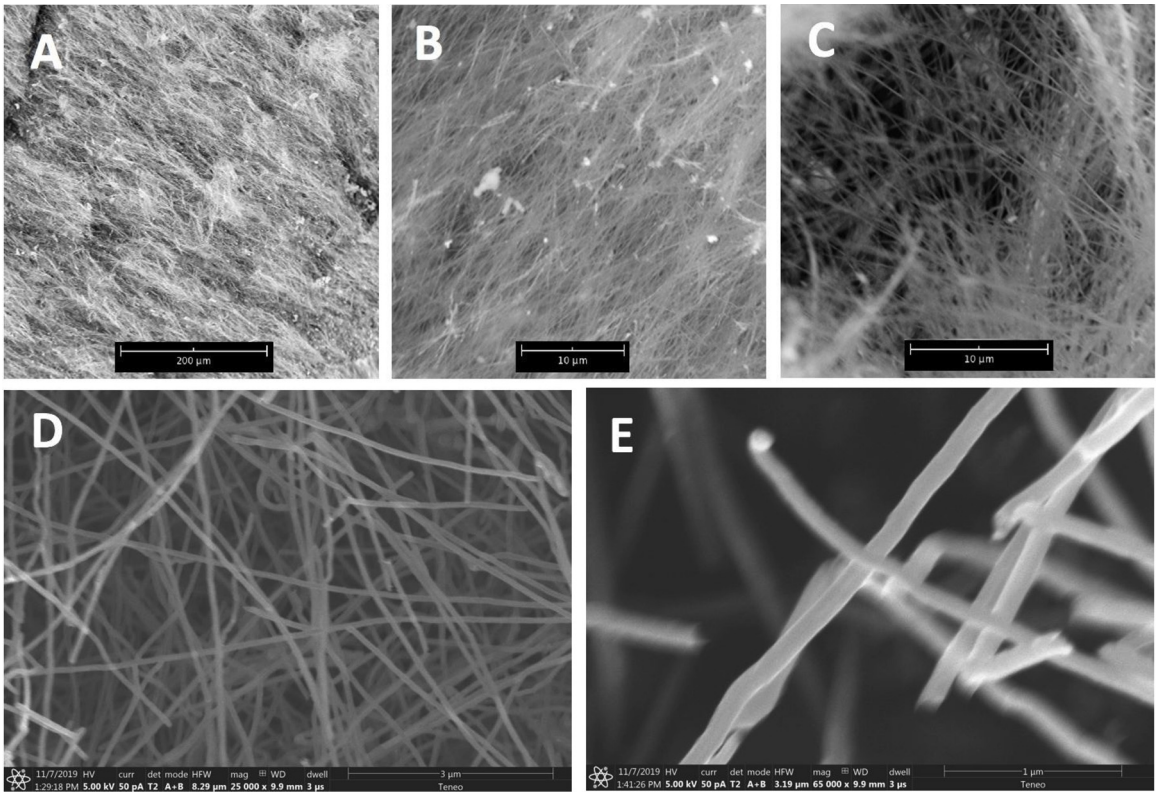


**Fig. 3.** SEM (panels A-C) and high resolution SEM (panels D and W) of the CNT product of $CO_2$ splitting in a molten Li carbonate electrolyte containing 2 wt% lithium oxide. The scale bars in the SEM A-C are respectively at 200, 10, and 10 µm. The scale bars in the SEM D and E are respectively at 3 and 1 µm.

nucleation of carbon to grow CNTs. While an additional mechanism of CVD CNT growth via the ability of carbides to dissolve carbon and thereby nucleate growth had been observed, it had not been evident or contemplated that such an alternative mechanism might apply to the electrochemical environment of the C2CNT process.

Iron carbide, $Fe_3C$, is an intermediate transition metal carbide. It is ferromagnetic, and begins to decompose to graphitic carbon and γ–iron at temperatures above 723 °C. The study of iron carbide, nucleated CNT growth in CVD has been widely explored, as well as the related CVD growth of graphene encapsulated iron carbide nodules on the CNT walls, and iron and iron carbide filling within the CNTs [47–56]. Within the CVD grown CNT, the iron carbide exhibits a lattice separation of ~0.2 nm compared to twice that for graphitic structures [57] Other carbon nanomaterials and nanographitic structures, including graphene, spheroids and nanocapsules, have also been grown by CVD with iron carbide [58–64]. Other metal carbides, principally cobalt and nickel carbide, but potentially also zirconium, tantalum and hafnium, can also nucleate CNT and other carbon nanomaterial growth in CVD [65–69]. Mechanisms of a non-metal carbides, silicon carbide, SiC, CVD formation of CNTs have also been explored and demonstrated [70,71]. While Ge + C may not thermodynamically form stable carbide phases, phases containing nano-germanium and carbon can form in carbide like phases. Ge nucleated CVD CNTs growth has also been reported [72–75], and the properties of germanium carbide, $Ge_xC_{1-x}$, have been investigated [76,77], and while the two have not been linked, in a manner analogous to the silicon carbide effect, germanium carbide mediated CNT growth is a possibility.

Carbon nanomaterials containing iron carbide or other ferromagnetic magnetic materials such as iron or magnetite are attracted to magnets and have been of growing interest for a wide range of fields including medicine and catalysis. There has been a wide range of interest in magnetic CNTs in medical applications as a tool for targeted drug delivery and imaging, in fields including MRIs, stem cells, and anticancer agents for the colon, lymph nodes, melanoma and bladder [78–90]. For catalyst applications, the magnetic properties allowing for recoverable nano and dendritic materials is a growing field of interest [91–96]. Specific applications include magnetic CNTs [97–100], magnetic graphene [101–104], and magnetic carbon sphere and nano-onion catalysts [105–108].

Here, the first ferromagnetic CNTs produced from $CO_2$ by the C2CNT process are observed; leading to a search and discovery of a carbide, rather transition metal, nucleation of the C2CNT process. On a practical note, $CO_2$ electrolysis in a cast iron case leads to highly uniform, high coulombic efficiency, and high aspect ratio CNTs.

## 2. Experimental section

Lithium carbonate ($Li_2CO_3$, 99.5 %), and lithium oxide ($Li_2O$, 99.5 %), are combined to form various molten electrolytes.

Electrolyses are driven at 0.5 A (amp) current at a constant current density as described. The electrolysis is contained in a pure stainless steel 304 case or cast iron pot. Inconel 718, Nichrome, or Incoloy was the (oxygen generating) anode, and Muntz brass as the cathode. During electrolysis, the carbon product accumulates at the cathode, which is subsequently removed and cooled. After electrolysis the product remains on the cathode but falls off or peels off when the cathode is extracted, cooled, and tapped. The product is washed with either DI water or up to 6 m HCl (both yield similar product, but the latter solution accelerates washing), and separated from the washing solution by either paper filtration or centrifugation (both yield similar product, but the latter accelerates the separation).

### 2.1. Characterization

The carbon product is washed, and analyzed by PHENOM Pro Pro-X SEM (with EDS), FEI Teneo LV SEM, and by FEI Teneo Talos F200X TEM. XRD powder diffraction analyses were conducted with a Rigaku Miniflex diffractometer and analyzed with the Jade software package.

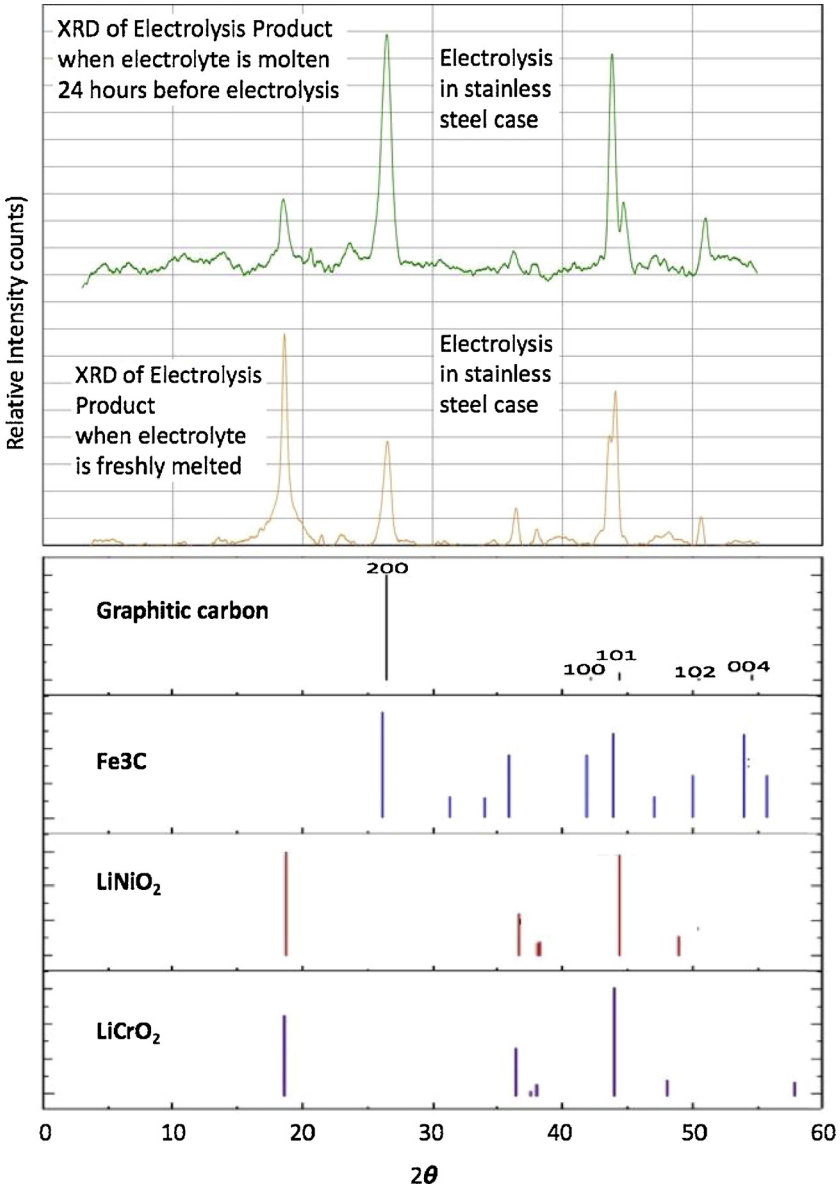


**Fig. 4.** XRD of the cathode product of electrolyses conducted under similar configuration, but in one case (XRD A) the electrolyte was held molten for 1 day prior to immersion of the electrodes and start of the electrolysis, and in the second case (XRD B) the electrolysis was conducted when the electrolyte was freshly melted. Both electrolyses were conducted for 4 h in a stainless steel 304 case, and utilized a 770 °C $Li_2CO_3$ electrolyte with 2 wt% added $Li_2O$, with a brass cathode and a nichrome anode.

## 3. Results and discussion

The reduction of $CO_2$ in lithiated carbonate electrolytes is a 4 $e^-$ (electron) process:

$$Li_2CO_{3(molten)} + 4e\text{-} \rightarrow C_{(nanomaterial;)} + O_{2(gas)} + Li_2O_{(dissolved)} \quad (2)$$

$CO_2$ added to the electrolyte chemically reacts with lithium oxide to renew and reform $Li_2CO_3$: $CO_{2(atmospheric\ or\ stack)} + Li_2O_{(dissolved)} \rightleftharpoons Li_2CO_{3(molten)}$ (3)

Eq 2 combined with Eq 3 yields the net electrolysis reaction:

$$CO_{2(gas)} + 4e^- \rightarrow C_{(nanomaterial)} + O_{2(gas)} \quad (4)$$

Lithium carbonate melts at 723 °C. At temperatures higher than 800 °C, a two, rather four, electron reduction increasingly dominates, and by 950 °C, the electrolysis product is pure carbon monoxide, rather than carbon [109]:

$$CO_{2(gas)} + 2e^- \rightarrow CO_{(gas)} + 1/2\ O_{2(gas)} \quad (5)$$

Fig. 1A presents the electrolysis of pure $CO_2$ gas bubbled into molten lithium carbonate with and without 1 m lithium oxide (1 mol $Li_2O$ per kg $Li_2CO_3$) added to the electrolyte as reported in reference [34]. As seen in the middle panel, after a brief period of activation, the gas phase portion of the electrolysis product rises in time to 100 % oxygen and no $CO_2$ escapes the electrolysis. The electrolysis is conducted in the stainless steel 304 case shown, and internally the anode is Inconel 718 and the cathode is Muntz brass [34]. In accord with Eq 4, a carbon nanomaterial product grows on the cathode, and after cooling and washing, the carbon nanomaterial is found to be CNTs. Specifically, after the synthesis the extracted cathode is cooled, the solid product is readily peeled off the cathode and washed to remove excess electrolyte. Unexpectedly, when the electrolysis is conducted in an iron containing case, the product is these magnetic carbon nanomaterials. Here, as shown in Fig. 1B, and as reported for the first time, the electrolytically grown CNTs are ferromagnetic and strongly attracted to a magnet.

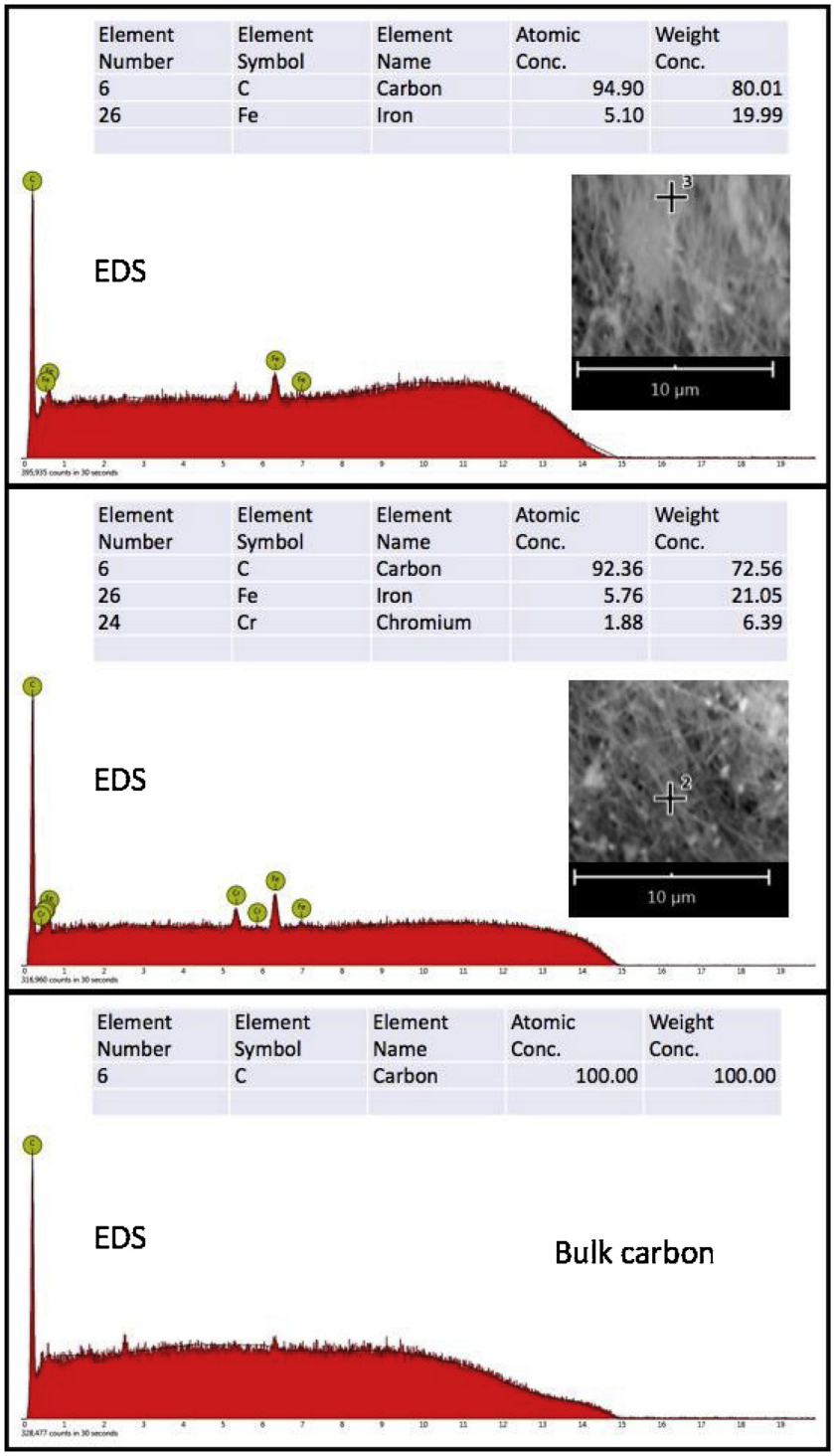


**Fig. 5.** EDS of the washed cathode product of an electrolysis for 4 h at 0.2 A $cm^{-2}$ in a stainless steel 304 case, which utilized a 770 °C $Li_2CO_3$ electrolyte with 2 wt% added $Li_2O$, with a brass cathode and a nichrome anode.

Molten $Li_2CO_3$ has a strong affinity for $CO_2$, and the electrolysis is effective using airborne $CO_2$ (direct air carbon capture of the 216 ppm in the air, without $CO_2$concentration), rather than pure $CO_2$ gas. The basic morphology of the C2CNT grown CNTs is the same whether grown in ceramic (alumina) or steel electrolysis cases. The observed exception will be shown in the last example when excess iron is introduced from the anode or case during the electrolysis. SEM Fig. 2A shows the highly uniform CNT product using $CO_2$ from the air as the reactant, as previously described and again using an Inconel 718 anode and a Muntz brass cathode. The molten $Li_2CO_3$ electrolyte has been exposed to (hot) air 24-hr prior to the electrolysis [34]. Fig. 2B and C use TEM to show the CNT walls, and that the graphene spacing between the CNT walls is the expected 0.33 to 0.34 nm.

Magnetic CNTs, such as those shown in Fig. 3, can be grown even when the anode contains no iron. This electrolysis was conducted using a Nichrome A (composed of 80 % nickel and 20 % chromium) anode and a Muntz brass (composed of 60 % copper and 40 % zinc) cathode in molten $Li_2CO_3$ containing 0.67 m $Li_2O$. Fig. 3 presents SEM of the CNTs grown in 770 °C $Li_2CO_3$ with 2 wt% Li oxide electrolyte at a constant current density 0.1 A/$cm^2$ for 4 h using a nickel alloy anode and brass

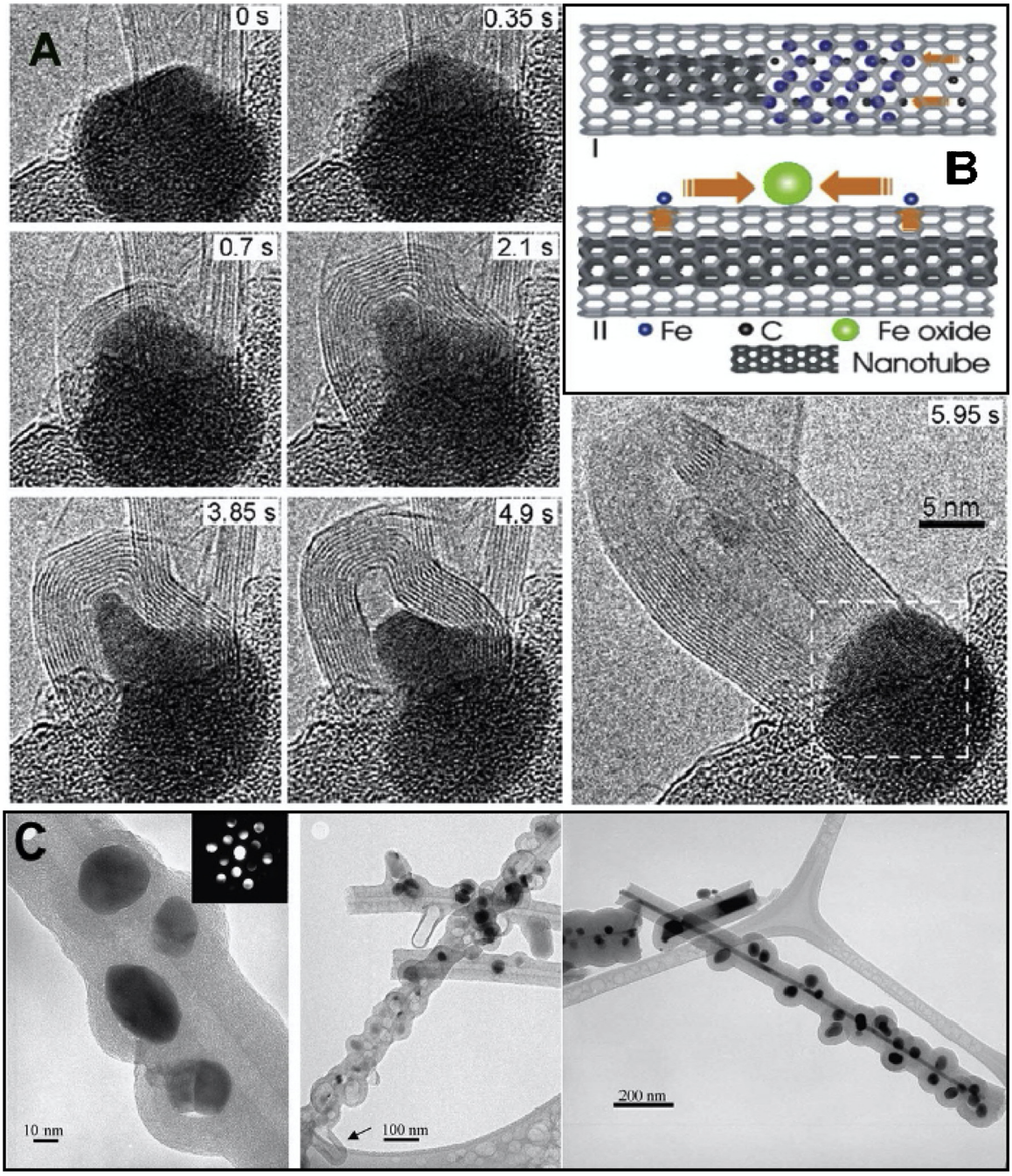


**Fig. 6.** A) Nucleation and CVD growth of a MWCNT from an iron carbide nanoparticle on a silicon substrate as observed by ref. [38]. Graphene layers are formed on the iron carbide and then an MWCNT is suddenly expelled from the deformed iron carbide particle. B) The proposed catalytic reaction for the inner-tube growth by CVD. I) The iron carbide nanocrystal is acting as a reactor absorbing carbon atoms from one side and generating a nanotube to another side. II) Proposed movement of iron atoms and oxidation and aggregation proposed by ref. [39]. C) CNTs with nodules grown from ferrocene vapor [45]. Figured 3A, B and C are respectively modified with permission from references [38,[39 and 45.

cathode. Nickel and chromium alloy anodes and brass cathodes have been shown to be particularly stable for repeated use in $CO_2$ splitting by molten carbonate electrolysis [14]. The electrolysis chamber walls can be lined with nickel or a nickel alloy to further decrease iron release from the cell walls into the cell. After the synthesis, the extracted cathode is cooled, and the solid product readily is peeled off the cathode and washed to remove excess electrolyte prior to microscopy. The product is ~98 % uniform CNTs as determined by visual inspection of multiple SEMs and the TEM. The coulombic efficiency approaches 100 % during this electrolysis. The coulombic efficiency of electrolysis is the percent of applied, constant current charge that was converted to carbon determined as:

$$100\ \%\ \text{x}\ C_{experimental}\ /\ C_{theoretical} \quad (6)$$

This is measured by the mass of washed carbon product removed from the cathode, $C_{experimental}$, and calculated from the theoretical mass, $C_{theoretical}$ = (Q/nF) x (12.01 g C $mol^{-1}$) which is determined from Q, the time-integrated charged passed during the electrolysis, F, the Faraday (96485 As $mol^{-1}$ $e^{-}$), and the n = 4e- $mol^{-1}$ reduction of tetravalent carbon.

Fig. 4 presents XRD of two different products of electrolyses conducted in stainless steel 304 cases. XRD A is diffraction spectra of the

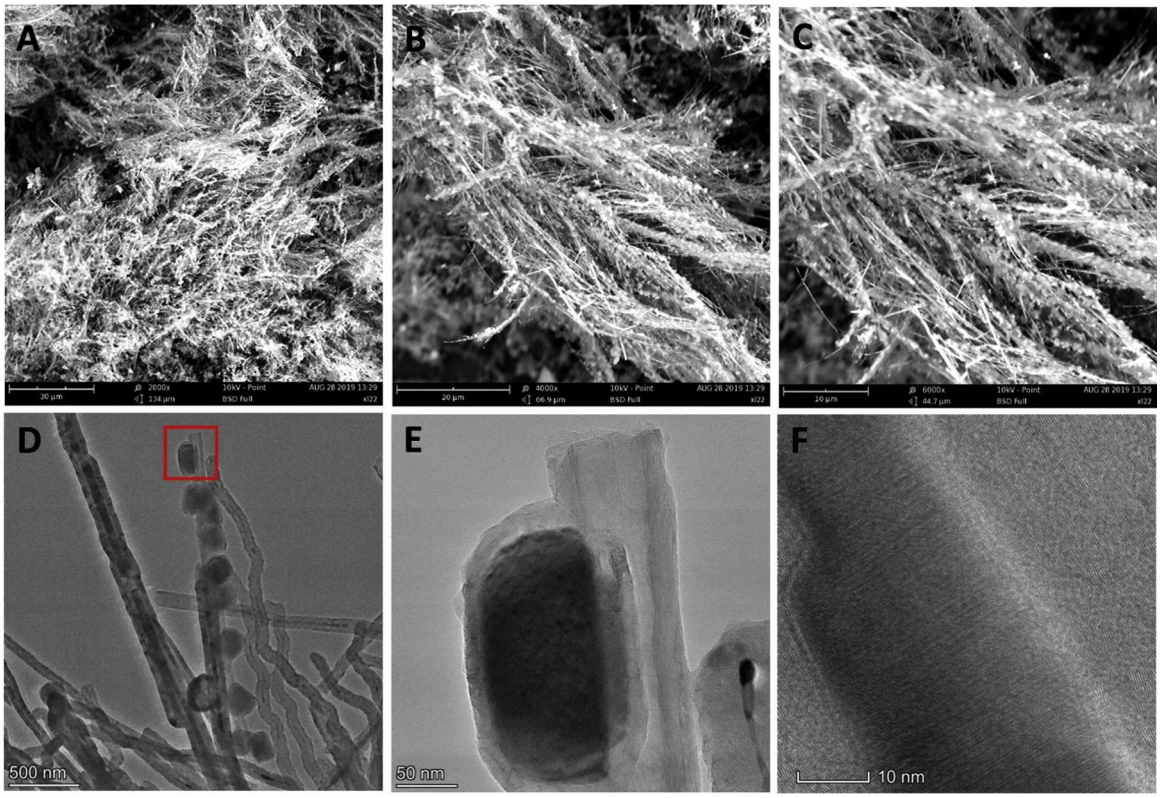


**Fig. 7.** C2CNT grown MWCNT with a high iron content anode can exhibit nodules on the CNT. SEM (panels A-C) and TEM (panels D-F) of the CNT product of $CO_2$ splitting in molten Li carbonate electrolyte oxide. SEM: The scale bars in A-C are respectively 30, 20, and 10 μm. SEM: The scale bars in D-F are respectively 500, 50, and 10 nm.

product of an electrolysis conducted after the electrolyte has sat molten in the case for 24 h. XRD B is of the product of an electrolysis conducted with freshly melted electrolyte. The bottom of the figure comprises a library XRD of compounds relevant to the product (graphitic carbon, iron carbide, and nickel lithium oxides or chromium lithium oxides). XRD A exhibits evidence of significantly more iron carbide in the graphitic carbon product than XRD B. While the electrolysis case had no visible sign of corrosion after either electrolysis, it is evident that the long electrolyte soak prior to the electrolysis and XRD A of the product resulted in greater iron carbide in that product. Significant peaks are observed at 2Ø of x = 19°, y = 26°, and z = ~44°. Specifically, as compared to the XRD library in the lower portion of the figure, both XRDs exhibit either chromium or nickel oxide peaks at x and z, and both XRD exhibit graphitic peaks at y. However, the ratio of the peaks in the XRD A, which is the relative height of peak z to either peak x or y compared to XRD B, shows the strong contribution of the iron carbide spectra at y and z. Furthermore, at "z" (~44°) there is an evident doublet peak. In XRD A the dominance of the left peak compared to either the right peak, and the dominance of that peak compared to the peak at "x" (19°), is consistent with the contribution of the iron carbide diffraction spectrum. EDS of sample A, as shown in Fig. 5, is consistent with the XRD results, showing an elemental analysis at three spots on the CNT product a point that is 100.0 % atomic percent C, a point that is 94.9 % C and 5.1 % Fe, and a point that is 92.4 % C, 5.8 % Fe and 1.9 % Cr. While the source of the iron producing the carbide is evidently from the electrolysis chamber walls, it is evident that alternate sources can be from oxidation of a component of the anode (for iron containing anodes), as a direct additive to the electrolyte, or from a component of the cathode (for iron containing cathodes). EDS is an elemental analysis an incapable of discerning between metallic iron and iron carbide (or chromium carbide) at the carbon nanotubes. However, the XRD of Fig. 4 definitively establish the presence of iron carbide, As observed in a different synthetic process (the chemical gas/solid phase and dilute carbon source) of CVD, we are likely observing a dynamic range of iron metal to iron carbide compositions which varies with CNT growth as enumerated for CVD in the next paragraph, and as will be the topic of future electrochemical investigations.

Despite the difference in physical chemical environments, the novel iron carbide occurrences and processes observed in the electrochemical deposition C2CNT process, exhibit several mechanistic and physical chemical behaviors analogous to those seen previously in chemical vapor deposition. In a CVD nucleation process from iron particles embedded in silicon, as seen in Fig. 6A, Yoshida et al. have observed CVD growth in real-time (t, the time is shown in the figure panels) of CNTs, The structure of the iron carbide nucleation particles is seen to fluctuate in time, and when discussing multiwalled CNTs (MWNTs) from nanoparticle catalysts (NPCs) the researchers state: "In the nucleation process of a MWNT, graphene layers are first formed on a facet of a NPC, as seen in the Fig. 2 (t 0 s). As is noted above, individual graphene layers can be clearly observed. The graphene layers gradually extend and bend along the facets of the NPC (t 0.35 s), and additional graphene layers nucleate beneath the existing ones. Accordingly, the NPC is gradually deformed (t 0.7 s), forming the characteristic protrusion (t 2.1 and 3.85 s). The NPC expels a MWNT suddenly, exhibiting the facet at the tip of its protrusion (t 4.9 s), and this MWNT grows rapidly (from t 4.9–5.95 s). Naturally, this root-grown MWNT is encapsulated at the tip." [49]. A mechanism for iron carbide mediated CVD growth of a wall within a CNT wall has been proposed by Shiozawa *et al.* [50] and is summarized in Fig. 6B as an iron carbide nanocrystal acting as a reactor absorbing carbon atoms from one side and generating a nanotube to another side. As summarized in Fig. 6C Liu et al. have observed graphite coated iron carbide nodules both on and within CNTs grown from ferrocene (melting point 172.5 °C and boiling point 249 °C) in the vapor phase at 1000 °C and higher in enclosed quartz capsules [56].

Fig. 7 presents an experiment in which the electrolysis is purposely conducted in an environment that contains an excess of iron.

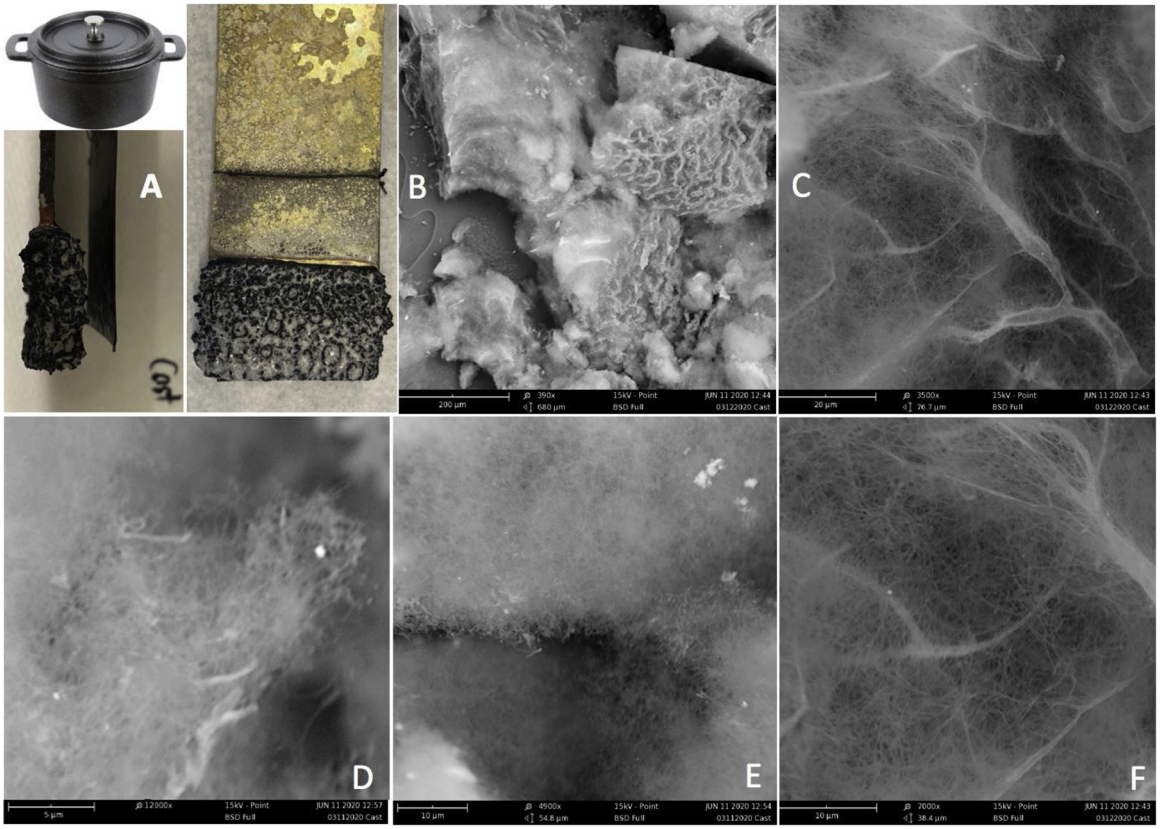


**Fig. 8.** Cast iron pot synthesis of CNTs from $CO_2$ with 20 $cm^2$ brass cathode and nichrome anode at a constant current of 0.1 A/$cm^2$ in 770 °C L for 4 h. A: The small (10 cm diameter x5 cm height) cast iron pot used in the synthesis (without the cover). $Li_2CO_3$ is heated inside the pot overnight to remove the surface layer (and then replaced with 300 g of fresh $Li_2CO_3$ as the electrolyte, and is without additives). After the electrolysis, the electrodes are extracted and cooled; the brass cathode with carbon product and the nichrome anode are shown on the left, and the front view of the cathode is adjacent. SEM of the washed product is shown with scale bars. B:200 μm, C:20 μm, D:5 μm, E & F: 10 μm.

Specifically, rather than a nichrome anode, the electrolysis includes an anode that contains an Incoloy alloy that is composed of over 40 % iron, 30–35 % nickel and 19–23 % chromium. The electrolysis is still conducted in a stainless steel case. With this high content of iron, the anode may release excess iron oxide during the electrolysis, and in this electrolysis in $Li_2CO_3$ at 0.1 A/$cm^2$, the measured coulombic efficiency drops to 89 %. SEM and TEM of the electrolysis product are shown in Fig. 7, and unlike the CNTs in Figs. 2 and 3, graphene-coated nodules are seen to grow on the outside of the CNTs and the interiors of the CNTs are partially filled with a deposit. Similar, nodules and filling have been observed in CVD grown in iron carbide driven CNT growth and the interior of the nodules and the CNT filling identified as iron carbide [47,49,56–58]. As presented in the TEM Fig. 7F of the excess iron electrolysis product, the inter-lattice distance between the layers is only 0.20 nm, which is significantly smaller than the graphene inter-lattice layer of 0.33 to 0.34 nm between the CNT graphene walls. This is 0.20 nm inter-lattice separation has previously been identified as iron carbide [57,63,64].

We have observed that an electrolysis conducted in a $Li_2CO_3$ electrolyte with a low concentration of added $Li_2O$, or an electrolyte aged for 24 h can lead to a higher yield of uniform CNTs, than an equivalent pure $Li_2CO_3$ electrolyte that has not been aged. This leads to the novel idea in Fig. 7 that an electrolysis with pure $Li_2CO_3$ electrolyte that has not been aged, but is conducted in a cast iron (iron that contains 2–4.3 % carbon), rather than stainless steel case, may promote iron carbide formation of graphitic structures and lead to a more uniform electrolysis product. Cast iron pot synthesis of CNTs from $CO_2$ with 20 $cm^2$ Muntz brass cathode and nichrome anode at a constant current of 0.1 A/$cm^2$ in 770 °C L for 4 h was conducted and the product is shown in Fig. 8. The CNTs are highly uniform and have a high aspect (length to diameter) ratio. The coulombic efficiency, as measured by Eq. 6, approached 100 % and the product was uniform (~98 % pure) ultrathin CNTs.

## 4. Conclusions

Here, the first ferromagnetic CNTs produced from $CO_2$ by the C2CNT process are observed. This observation leads to the search and discovery of a carbide, rather transition metal, nucleation of the carbon nanotube electrolysis growth process. $CO_2$ can be split by molten carbonate electrolysis to grow magnetic carbon nanotubes (MCNTs). This opens the path to other similar electrochemically prepared magnetic carbon nanomaterials.

In the presence of an iron or nickel containing case to house the molten carbonate electrolysis, or the presence of Fe or Ni in the anode, ferromagnetic CNTs can grow at the cathode. For example, EDS elemental analysis confirms the presence of iron in the CNTs, and XRD confirms the presence of iron carbide at the CNT nucleation site. The observed interlattice spacing of 0.20 nm of the iron carbide is distinct from the observed 0.36 nm graphene lattice spacing of the CNT walls. An excess iron release can be accomplished into the electrolyte using an iron rich alloy anode, such as Incoloy, and the excess iron results in graphene layer coated iron carbide nodules on the exterior of the carbon nanotube product formed at the cathode, as well as iron carbide within these CNTs as observed by SEM and TEM.

On a practical note, $CO_2$ electrolysis in a cast iron case leads to highly uniform, high coulombic efficiency, and high aspect ratio MCNTs. Magnetic carbon nanomaterials have a variety of applications, such as in directing medical therapy to localized regions and recoverable catalysts. On a second practical note, the new production of

magnetic carbon nanotube is substantially more cost-effective and green house gas mitigating than those grown by conventional CVD. The electrolysis costs are similar to those in well-established aluminum production by electrolysis, a cost that is two orders of magnitude less expensive than CVD [32,33].

## Declaration of Competing Interest

The authors declare no conflict of interest.

## Acknowledgements

We are grateful to C2CNT for support of this research.

## References

[1] K.S. Novoselov, A.K. Geim, S.V. Morzov, D. Jiang, Y. Zhang, S.V. Dubonos, I.V. Grigorieva, A.A. Firsov, Electric field effect in atomically thin carbon films, Science 306 (2004) 666.
[2] W. Tian, W. Li, W. Yu, X. Liu, Micromachines 8 (163) (2017) 1.
[3] M.-F. Yu, O. Lourie, M. Dyer, K. Moloni, T. Kelly, R. Ruoff, Science 287 (2000) 637.
[4] C.-C. Chang, H.-K. Hsu, M. Aykol, W. Hung, C. Chen, S. Cronin, ACS Nano 4 (2010) 5095.
[5] S. Licht, X. Liu, G. Licht, X. Wang, A. Swesi, Y. Chan, Mater. Today Sustainabl. 6 (2019) 100023.
[6] J. Kaur, G.S. Gill, K. Jeet, Applications of carbon nanotubes in drug delivery: a comprehensive review, Characterization and Biology of Nanomaterials for Drug Delivery, (2019), p. 113 Chapter 5.
[7] H. Yang, W. Xu, X. Liang, Y. Yang, Y. Zhou, Carbon nanotubes in electrochemical, colorimetric, and fluorimetric immunosensors and immunoassays: a review, Microchim. Ichnoanal. Acta 187 (2020) 20.
[8] H.K. Moghaddam, M.R. Maraki, A. Rajaei, Application of carbon nanotubes(CNT) on the computer science and electrical engineering: a review, Int. J. Reconfigur. Embedded Syst. (IJRES) 9 (2020) 61.
[9] S. Licht, A. Douglas, R. Carter, M. Lefler, C. Pint, ACS Cent. Sci. 2 (2015) 162.
[10] P. Sehrawat, C. Julien, S.S. Islam, Carbon nanotubes in Li-ion batteries: A review, Mater. Sci. Eng. B 213 (2016) 12.
[11] L. Sun, X. Wang, Y. Wang, Q. Zhang, Roles of carbon nanotubes in novel energy storage devices, Carbon 122 (2017) 462.
[12] R. Seman, M. Azam, A. Mohamad, Systematic gap analysis of carbon nanotube-based lithium-ion batteries and electrochemical capacitors, Renew. Sustain. Energy Rev. 75 (2017) 644.
[13] T. Han, A. Nag, S.C. Mukhopadhyay, Y. Xu, Carbon nanotubes and its gas-sensing applications: a review, Sens. Actuators A Phys. 291 (2019) 107.
[14] S. Kumar, V. Pavelyev, N. Tripathi, V. Platonov, P. Sharma, R. Ahmad, P. Mishra, A. Khosla, Review—recent advances in the development of carbon nanotubes based flexible sensors, J. Electrochem. Soc. 167 (2020) 047506.
[15] Z. Abdullah, A. Othman, S. Mwabaidur, Application of carbon nanotubes in extraction and chromotographic analysis: a review, Arab. J. Chem. 12 (2019) 633.
[16] B.V. Basheer, J. George, S. Siengchin, J. Parameswaranpillai, Polymer grafted carbon nanotubes—synthesis, properties, and applications: a review, Nano-Struct. Nano-Objects 22 (2020) 100429.
[17] S. Imtiaza, M. Siddiqa, A. Kausara, S. Munthaa, J. Ambreenb, I. Bibic, A review featuring fabrication, properties and applications of carbon nanotubes (CNTs) reinforced polymer and epoxy nanocomposites, Chin. J. Polym. Sci. 36 (2018) 445.
[18] S. Gantayata, D. Routb, S.K. Swain, Carbon nanomaterial–reinforced epoxy composites: a review, Polym. Technol. Eng. 57 (2018) 1.
[19] I. Rafiquea, A. Kausara, Z. Anwara, B. Muhammad, Exploration of epoxy resins, hardening systems, and Epoxy/Carbon nanotube composite designed for high performance materials: a review, in: A. Kausara, I. Rafiquea, B. Muhammad (Eds.), Review of Applications of Polymer/Carbon Nanotubes and Epoxy/CNT Composites, 55 2016, p. 312 ibid 1167.
[20] S. Shahidi, B. Moazzenchi, Carbon nanotube and its applications in textile industry – a review, J. Text. Instit. 109 (2018) 1653.
[21] Su. Rather, Preparation, characterization and hydrogen storage studies of carbon nanotubes and their composites: a review, Int. J. Hydrogen Energy 45 (2020) 4653.
[22] M. Selvaraja, A. Haia, F. Banata, M. Haijab, Application and prospects of carbon nanostructured materials in water treatment: a review, J. Water Process Eng. 33 (2020) 100996.
[23] M. Bassyouni1, A.E. Mansi, A. Elgabry, B.A. Ibrahim, O.A. Kassem, R. Alhebeshy, Utilization of carbon nanotubes in removal of heavy metals from wastewater: a review of the CNTs' potential and current challenges, Appl. Phys. A 126 (2020) 1.
[24] M. Ghoranneviss, A.S. Elahi, Mol. Cryst. Liq. Cryst. 629 (2016) 158.
[25] K.A. Shah, B.A. Tali, Mater. Sci. Semiconduct. Process. 41 (2016) 67.
[26] V. Khanna, B.R. Bakshi, L.J. Lee, J. Ind, Ecology 12 (2008) 394.
[27] S. Licht, United States Patent Application Publication (2016) Pub. No.: US2016/00006090 A1.
[28] J. Ren, F.-F. Li, J. Lau, L. Gonzalez-Urbina, S. Licht, Nano Lett. 15 (2015) 6142.
[29] J. Ren, S. Licht, Sci. Rep. - Nature.com 6 (27760) (2016) 1.
[30] J. Ren, J. Lau, M. Lefler, S. Licht, J. Phys. Chem. C 119 (2015) 23342.
[31] S. Licht, et al., J. CO2 Util. 18 (2017) 335.
[32] M. Johnson, J. Ren, M. Lefler, G. Licht, J. Vicini, X. Liu, S. Licht, Mater. Today Energy 5 (2017) 230.
[33] M. Johnson, J. Ren, M. Lefler, G. Licht, J. Vicini, S. Licht, Data on SEM, TEM and Raman Spectra ofd oped, and wool carbon nanotubes made directly from CO2 by molten electrolysis, Data Brief 14 (2017) 592.
[34] X. Wang, X. Liu, G. Licht, B. Wang, S. Licht, J. CO2 Util. 18 (2019) 378.
[35] X. Liu, X. Wang, G. Licht, S. Licht, J. CO2 Util. 36 (2020) 288.
[36] X. Liu, J. Ren, G. Licht, X. Wang, S. Licht, Adv. Sustain. Syst. 1900056 (2019) 1.
[37] J. Ren, A. Yu, P. Peng, M. Lefler, F.-F. Li, S. Licht, Recent advances in solar thermal electrochemical process (STEP) for carbon neutral products and high value nanocarbons, Acct. Chem. Res. 52 (2019) 1871.
[38] Z. Li, G. Wang, W. Zhang, Z. Qiao, H. Wu, Carbon nanotubes synthesis from CO2 based on the molten salts electrochemistry: effect of alkaline earth carbonate additives on the diameter of the carbon nanotubes, Sustain. Energy Fuels 166 (2019) 2604.
[39] A. Fuente-Cuesta, C. Savinu, G. Carins, D. Miller, M. Lenzi, J. Irvine, Simultaneous CO2 removal from biomass conversion product gas and carbon nanotube formation via catalytic chemical vapour deposition, J. Electrochem. Soc. 166 (2019) D415.
[40] L. Hu, Y. Song, J. Ge, J. Zhu, Z. Han, S. Jiao, Electrochemical deposition of carbon nanotubes from CO2 in CaCl2–NaCl-based melts, J. Mater. Chem. A 5 (2017) 6219.
[41] Z. Li, D. Yuan, H. Wu, W. Li, D. Gu, A novel route to synthesize carbon spheres and carbon nanotubes from carbon dioxide in a molten carbonate electrolyzer, Inorg. Chem. Front. 5 (2018) 208.
[42] S. Mori1, N. Matsuura1, L.-L. Tun, M. Suzuki, Direct synthesis of carbon nanotubes from only CO2 by a hybrid reactor of dielectric barrier discharge and solid oxide electrolyser cell, Plasma Chem. Process. 36 (2016) 231.
[43] G. Simate, K. Moothi, M. Meyyappan, S. Lyuke, S. Ndlovu, R. Falcon, M. Heydenrych, Kinetic model of carbon nanotube production from carbon dioxide in a floating catalytic chemical vapour deposition reactor, RSC Adv. 4 (2014) 9564.
[44] G. Simate, S. Lyuke, S. Ndlovu, C. Yah, L. Alubita, The production of carbon nanotubes from carbon dioxide challenges and opportunities, J. Nat. Gas Chem. 19 (2010) 453.
[45] W. Wei, D. Stacchiola, Y. Hu, 3D graphene from CO2 and K as an excellent counter electrode for dye-synthesized solar cells, Energy Res. 9 (2017) 2502.
[46] A. Strudwick, N. Weber, M. Schwab, M. Kettner, R. Weitz, J. Wunsch, H. Sachdev, Chemical vapor deposition of high quality graphene films from carbon dioxide atmospheres, ACS Nano 41 (2015) 2502.
[47] L.C. Qin, CVD synthesis of carbon nanotubes, J. Mat. Sci. Lett. 16 (1997) 457.
[48] G. Gulino, R. Vieira, J. Amadou, P. Nguyen, M.J. Ledoux, G. S.Galvagno, C. Centi, Pham-Huu, C H as an active carbon source for a large scale synthesis of carbon nanotubes by chemical vapour deposition, Appl. Catal. A Gen. 2005 (2005) 89.
[49] H. Yoshida, S. Takeda, T. Uchiyama, H. Kohno, Y. Homma, Atomic-scale in-situ observation of carbon nanotube growth from solid state Iron carbide nanoparticles, Nano Lett. 8 (2008) 2082.
[50] H. Shiozawa, T. Pichler, A. Gruneis, R. Pfeiffer, H. Kuzmany, Z. Liu, K. Suenaga, H. Kataura, A catalytic reaction inside a single-walled carbon nanotube, Adv. Mater. 20 (2008) 1443.
[51] F.S. Boi, et al., The origin of long-period lattice spacings observed in iron-carbide nanowires encapsulated by multiwall carbon nanotubes, Microsc. Microanal. 19 (2013) 1.
[52] J. Shi, Y. Wang, W. Du, Z. Hou, Synthesis of graphene encapsulated Fe C in carbon nanotubes from biomass and its catalysis application, Carbon 199 (2016) 330.
[53] C. Wang, J. Kang, P. Liang, H. Zhang, H. Sun, M.O. Tadéa, S. Wang, Ferric carbide nanocrystals encapsulated in nitrogen-doped carbon nanotubes as an outstanding environmental catalyst, Environ. Sci. 4 (2017) 170.
[54] F. Ding, Iron-carbide cluster thermal dynamics for catalyzed carbon nanotube growth, J. Vac. Sci. Tech. A 22 (2020) 1471.
[55] Y. Yao, L. Falk, R. Morjan, O. Nerushev, E. Campbell, Synthesis of carbon nanotube films by thermal CVD in the presence of supported catalyst particles. Part II - the nanotube film, J. Mat. Sci. Mat. Electron. 15 (2004) 583.
[56] S. Liu, R. Wehmschulte, A novel hybrid of carbon nanotubes/iron nanoparticles: iron filled nodule-containing carbon nanotubes, Carbon 43 (2005) 1550.
[57] C. Lv, Q. Yang, Q. Huang, Z. Huang, H. Xiaab, C. Zhang, Phosphorus doped single wall carbon nanotubes loaded with nanoparticles of iron phosphide and iron carbide for efficient hydrogen evolution, J. Mater. Chem. A 4 (2016) 13336.
[58] J. Qiu, Q. Li, Z. Wang, Y. Sun, H. Zhang, CVD synthesis of coal-gas-derived carbon nanotubes and nanocapsules containing magnetic iron carbide and oxide, Carbon 44 (2006) 2565.
[59] R. Sergiienko, E. Shibata, S. Kim, T. Kinota, T. Nakamura, Nanographite structures formed during annealing of disordered carbon containing finely-dispersed carbon nanocapsules with iron carbide cores, Carbon 47 (2009) 1056.
[60] Y. Homma, H. Liu, D. Takagi, Y. Kobayashi, Single-walled carbon nanotube growth with non-iron-group "Catalysts" by chemical vapor deposition, Nano Res. 2 (2009) 793.
[61] H. Jiang, et al., Iron carbide nanoparticles encapsulated in mesoporous Fe–N-Doped graphene-like carbon hybrids as efficient bifunctional oxygen electrocatalysts, ACS Appl. Mater. Interfaces 7 (2015) 21511.
[62] Z. Wu, X.-X. Xu, B.-C. Hu, H.-W. Liang, Y. Lin, L.-F. Chen, S.-H. Yu, Iron carbide nanoparticles encapsulated in mesoporous Fe-N-Doped carbon nanofibers for

efficient electrocatalysis, Angew. Chem. Int. Ed. 54 (2015) 8179.
[63] M. Xiao, J. Zhu, L. Feng, C. Liu, W. Xing, Meso/Macroporous nitrogen-doped carbon architectures with Iron carbide encapsulated in graphitic layers as an efficient and robust catalyst for the oxygen reduction reaction in both acidic and alkaline solutions, Adv. Mater. 27 (2015) 2521.
[64] Z.Y. Hu, J. Jensen, W. Zhang, L. Cleemann, W. Xing, N. Bjerrum, Q. Ling, Hollow spheres of Iron carbide nanoparticles encased in graphitic layers as oxygen reduction catalysts, Angew. Chem. Int. Ed. 53 (2014) 3675.
[65] M. Kusunoki, T. Suzuki, K. Kaneko, M. Ito, Formation of self-aligned carbon nanotube by surface decomposition of silicon carbide, Philos. Mag. Lett. 79 (1999) 153.
[66] M.N. Grobert, M. Terrones, A. J.Osborne, H. Terrones, W.K. Hsu, S. Trasobares, Y.Q. Zhu, J.P. Hare, H.W. Kroto, D.R. M.Walton, Thermolysis of C60 thin films yields Ni-filled tapered nanotubes, Appl. Phys. A 67 (1998) 595.
[67] A. Borjesson, K. Boulton, First principles studies of the effect of nickel carbide catalyst composition on carbon nanotube growth, J. Phys. Chem. C 114 (2010) 18045.
[68] V.K. Portnoi, A.V. Leonov, S.N. Mudretsova, S.A. Fedotov, Formation of nickel carbide in the course of deformation treatment of Ni–C mixtures, Phys. Met. Metallogr. 109 (2010) 153.
[69] Y. Kohigashi, H. Yoshida, Y. Homma, S. Takeda, Structurally inhomogeneous nanoparticulate catalysts in cobalt-catalyzed carbon nanotube growth, Appl. Phys. Lett. 105 (073108) (2014) 1.
[70] M. Kusunoki, J. Shibata, M. Rokkaku, T. Hirayama, Aligned carbon nanotube film self-organized on a SiC wafer, Jap. J. Appl. Phys. Lett. 37 (2008) L605.
[71] M. Kusunoki, T. Suzuki, T. Hirayama, N. Shibata, K. Kaneko, A formation mechanism of carbon nanotube films on SiC(0001), Appl. Phys. Lett. 77 (2000) 531.
[72] G.A. Domrachev, et al., MOCVD synthesis of germanium filled "Diamondlike" carbon nanotubes and microtubes from organogermanium precursors and their field-emission properties, Chem. Vap. Deposit. 12 (2006) 357.
[73] A. Capasso, E.R. Waclawik, S. Ruffell, A. Sgarlata, M. Scarselli, M. De Crescenzi, N. Motta, Carbon nanotube synthesis from germanium nanoparticles on patterned substrates, J. Non-Crystalline Solids 15 (2010) 1972.
[74] W. Tang, Y. Liu, C. Peng, M.Y. Hu, X. Deng, M. Lin, J.Z. Hu, K.P. Loh, Probing Lithium germanide phase evolution and structural change in a germanium-in-carbon nanotube energy storage system, J. Am. Chem. Soc. 137 (2015) 2600.
[75] F. Wang, Z. Liu, M. Li, Q.-D. Wang, Germanium-doped and germanium/nitrogencodoped carbon nanotubes with highly enhanced activity for oxygen reduction in alkaline medium, RSC Adv. 6 (2016) 72676.
[76] Z.T. Liu, J.Z. Zhu, N.K. Xuu, X.L. Zheng, Structure and Properties of Germanium Carbide Films Prepared by RF Reactive Sputtering in Ar/CH4, Jap. J. Appl. Phys. Lett. 36 (1997) 3625.
[77] C.A. Stephenson, et al., Band structure of germanium carbides for direct bandgap silicon photonics, J. Appl. Phys. 120 (053102) (2016) 1.
[78] F. Yang, D.L. Fu, J. Long, Q.X. Ni, Magnetic lymphatic targeting drug delivery system using carbon nanotubes, Med. Hypothesis Discov. Innov. Ophthalmol. 70 (2008) 765–767.
[79] F. Yang, J. Hu, D. Yang, J. Long, G. Luo, C. Jin, X. Yu, J. Xu, C. Wang, Q. Ni, D. Fu, Pilot study of targeting magnetic carbon nanotubes to lymph nodes, NanoMedicine 4 (2009) doi.org/10.2217/nnm.09.5.
[80] O. Vittorio, et al., Magnetic carbon nanotubes: a new tool for shepherding mesenchymal stem cells by magnetic fields, NanoMedicine 6 (2010) doi.org/10.2217/nnm.10.125.
[81] F. Yang, et al., Magnetic functionalised carbon nanotubes as drug vehicles for cancer lymph node metastasis treatment, Eur. J. Cancer 47 (2011) 1873–1882.
[82] A. Mosotti, A. Caporali, Preparation of magnetic carbon nanotubes (Mag-CNTs) for biomedical and biotechnological applications, Int. J. Mol, Sci. 24 (2013) 24619.
[83] A.A. Faraj, A.P. Shaik, A.S. Shaik, Magnetic single-walled carbon nanotubes as efficient drug delivery nanocarriers in breast cancer murine model- noninvasive monitoring using diffusion-weighted magnetic resonance imaging as sensitive imaging biomarker, Int. J. Nanomed. 10 (2015) 157.
[84] W. Ding, et al., Targeted Fe-filled carbon nanotube as a multifunctional contrast agent for thermoacoustic and magnetic resonance imaging of tumor in living mice, Int. J. Nanomed. 12 (2016) 235.
[85] S. Boncel, et al., Hybrids of iron-filled multiwall carbon nanotubes and anticancer agents as potential magnetic drug delivery systems - in vitro studies against human melanoma, Colon carcinoma, and Colon adenocarcinom, J. Nanomater. 2017 (2017) 1.
[86] M. Samadishadlou, et al., Magnetic carbon nanotubes preparation physical properties and applications in biomedicine, Artif. Cells Nanomed. Biotechnol. 46 (2017) 1314.
[87] Q. Hu, et al., Magnetic carbon nanotubes camouflaged with cell membrane as a drug T discovery platform for selective extraction of bioactive compounds from natural products, Chem. Eng. J. 364 (2019) 269.
[88] N. Suo, et al., Magnetic multiwalled carbon nanotubes with controlled release of epirubicin- an intravesical instillation system for bladder cancer, Int. J. Nanomed. 14 (2019) 1241.
[89] M. Moazzen, et al., Multi-walled carbon nanotubes modified with iron oxide and silver nanoparticles (MWCNT-Fe3O4/Ag) as a novel adsorbent for determining PAEs in carbonated soft drinks using magnetic SPE-GC/MS method, Int. J. Nanomed. 12 (2019) 476.
[90] M. Moazzen, et al., Magnetic Nanoparticles Mediated Cancer Hyperthermia, Smart Healthcare for Disease Diagnosis and Prevention, Chapter 16 (2020), p. 153.
[91] X.Y. Zhu, et al., Preparation of ferrite magnetic nano-catalysts and their applications in the field of resources and energy, Progress Chem. 31 (2019) 381.
[92] S.B. Chen, et al., Magnetic Fe3C@C nanoparticles as a novel cocatalyst for boosting visible-light-driven photocatalytic performance of g-C3N4, Int. J. Hydrogen Energy 44 (2019) 26970.
[93] M. Sibi, D. Verma, J. Kim, Magnetic Magnetic core shell nanocatalysts promising versatile catalysts for organic and photocatalytic reactions, Catal. Rev. Sci. Eng. (2019), https://doi.org/10.1080/01614940.2019.1659555.
[94] R. Dalpozzo, Magnetic nanoparticle supports for asymmetric catalysts, Green Chem. 27 (2015) 3671.
[95] D. Wang, C. Deraedt, J. Ruiz, D. Astuc, Magnetic and dendritic catalysts, Accts, Chem. Res. 48 (2015) 1871.
[96] L. Rossi, N. Costa, F. Silva, R. Wojcieszak, Magnetic nanomaterials in catalysis - advanced catalysts for magnetic separation and beyond, Green Chem. 16 (2014) 2906.
[97] X. Wen, et al., In situ preparation of magnetic nickel-containing functionalized carbon nanotubes to support palladium as a catalyst for the Heck reaction, Appl. Catal. A Gen. 591 (2020) 117405.
[98] P. Akbarzadeh, N. Koukabi, E. Kolvari, Polythiophene-functionalized magnetic carbon nanotube-supported copper(I) complex- a novel and retrievable heterogeneous catalyst for the "Phosphine- and Palladium-Free" Suzuki–Miyaura cross-coupling, Mol. Divers. (2019), https://doi.org/10.1007/s11030-019-10016-x.
[99] S. Rezaei, et al., Chemoselective reduction of nitro and nitrile compounds with magnetic carbon nanotubes-supported Pt(II) catalyst under mild conditions, Green Chem. 56 (2017) 12256.
[100] M. Zhang, J. Lu, J. Zhang, Z. Zhang, Magnetic carbon nanotube supported Cu (CoFe2O4/CNT-Cu) catalyst - a sustainable catalyst for the synthesis of 3-nitro-2-arylimidazo[1,2-a]pyridines, Green Chem. 78 (2016) 26.
[101] A. Sheoran, et al., Graphene based magnetic nanohybrids as promising catalysts for the green synthesis of beta-amino alcohol derivatives, J. Mol. Struct. 1204 (2020) 127522.
[102] M. Kooti, F. Kooshki, E. Nasir, Preparation and characterization of magnetic graphene nanocomposite containing Cu(proline)2 as catalyst for asymmetric aldol reactions, Res. Chem. Intermediat. 45 (2019) 2641.
[103] M. Tanhae, A. Mahjouboshki, R. Nejat, Three-dimensional graphene–magnetic palladium nanohybrid- a highly efficient and reusable catalyst for promoting organic reactions, Cat. Lett. 148 (2018) 1549.
[104] Z.F. Li, et al., Nano-Co3O4 supported on magnetic N-doped graphene as highly efficient catalyst for epoxidation of alkenes, Mol. Cat. 432 (2017) 267.
[105] T. Yin, R. Ma, Y. Gu, A. Wu, X. Zhou, C. Tian, Cluster-like Co4N embedded into carbon sphere as an efficient, magnetic-separated catalyst for catalytic hydrogenation, ChemistrySelect 4 (2019) 90.
[106] C. Zhang, J. Li, C. Shi, C. He, E. Liu, N. Zhao, Self-anchored catalysts for substrate-free synthesis of metal-encapsulated carbon nano-onions and study of their magnetic properties, Nano Res. 9 (2016) 1159.
[107] Y. Wang, H. Sun, H. Ang, M. Tade, S. Wang, Synthesis of magnetic core/shell carbon nanosphere supported manganese catalysts for oxidation of organics in water by peroxymonosulfate, J. Colloid Interf. Sci. 433 (2014) 68.
[108] S. Lin, C. Chen, D. Lu, C. Wang, H. Gao, Synthesis of Pt nanoparticles anchored on graphene-encapsulated Fe3O4 magnetic nanospheres and their use as catalysts for methanol oxidation, Carbon 53 (2013) 112.
[109] S. Licht, B. Wang, S. Ghosh, H. Ayub, D. Jiang, J. Ganleyk, A new solar carbon capture Process: solar thermal Electrochemical Photos (STEP) carbon capture, J. Phys. Chem. Lett. 1 (2010) 2363.